International Journal of Marine Engineering Innovation and Research, Vol. 10(3), Sept. 2025. 881-890
(pISSN: 2541-5972, eISSN: 2548-1479)

Numerical Study of Fillet Effects on Cavitation Development in Double Contraction Pipes

Ridwan Daris Naufal[1], Damora Rhakasywi [2*], Fahrudin [3]

(Received: 14 August 2025 / Revised: 20 August 2025 /Accepted: 22 August 2025 / Available Online: 22 September 2025)

***Abstract*— This study investigates the effects of fillet geometry on cavitation development in series pipe systems with double sudden contraction using numerical simulations. The research evaluates how variations in fillet radius at contraction joints and inlet flow rate affect pressure distribution and cavitation characteristics. Three pipes with diameters of D, 0.6D, and 0.4D were arranged in series, with flow rates ranging from 500 to 3000 l/min. Simulations were conducted using ANSYS Fluent with the k-ε turbulence model and Zwart-Gerber-Belamri cavitation model to predict vapor volume fraction and cavitation potential. Mesh independence verification ensured simulation accuracy. Results showed that the first contraction presented minimal cavitation risk, with cavitation number values above 0.5 across all conditions, while the second contraction showed significant cavitation, especially at higher flow rates. Increasing the fillet radius elevated local minimum pressure, reduced peak vapor fraction, and shortened the cavitation zone. Fillets helped smooth velocity gradients and reduce flow separation, lowering cavitation likelihood. These findings highlight the importance of geometric modification in minimizing cavitation and improving system durability. The study provides useful insights for designing more resilient industrial piping systems under high-flow conditions by combining flow control strategies and joint geometry optimization.**

Keywords—Cavitation, Sudden Contraction, Fillet Geometry, Pressure Drop.

[*]*Corresponding Author:rhakasywi@upnvj.ac.id*

I. INTRODUCTION

Cavitation is a common phenomenon in flow systems that experience significant pressure fluctuations, such as in nuclear power plant piping systems, aircraft fuel injection systems, pump systems, and flow measurement devices [1], [2], [3]. This phenomenon occurs due to a significant pressure drop to the saturated vapor pressure of the working fluid [4]. In the case of water as the working fluid, the pressure drop to the saturated vapor pressure causes the water to change phase from liquid to vapor at the same temperature [5]. In many cases, this phenomenon can result in severe damage, including pipe wall erosion, vibration, and decreased system efficiency [6]. The complexity of cavitation formation increases when the system consists of pipes joined in series with varying diameters, as changes in geometry significantly affect the pressure distribution and flow velocity [7]. Therefore, research on cavitation formation in series pipe connections needs to be studied comprehensively to improve the reliability and efficiency of industrial piping systems.

Research on flow behavior and cavitation phenomena in series pipes using computational methods has been conducted previously. X. Tang et al. (2020) [8] have conducted research using the Computational Fluid Dynamics (CFD) method based on a weakly compressible fluid model to investigate transient cavitation flow in pipes. The study introduced a fluid density-pressure model that describes the variable wave velocity of the transient cavitation flow. The simulation generates flow behavior information, including velocity, pressure, and vapor volume fraction, and analyzes the pressure wave propagation characteristics both qualitatively and quantitatively. The study found a significant role of the pressure waveform and pressure gradient on the intensity and length of the cavitation zone. Additionally, water hammer and transient cavitation phenomena occurred with the CFD model, which is based on a weakly compressible fluid. Thus, the simulation has demonstrated the complex interaction and dynamics between reflective pressure waves and bubble collapse.

Cavitation is affected by changes in pressure and flow geometry. Research by Lei et al. (2023) [9] revealed the relationship between the shape of the flow geometry passed through the cavitation formed in the sudden contraction pipe. The study examined the relationship between the shape of the transition section and the cavitation characteristics at the outlet of the bottom discharge tunnel. The study found that the four main factors that affect the risk of cavitation are the contraction ratio of the transition section, the top press slope, the length of the transition section, and the shape of the orifice. Designs with a high contraction ratio can increase the risk of cavitation. Therefore, curved profiles and longer transition sections can reduce the minimum pressure and avoid the pressure falling below the vapor pressure.

Research conducted by Fujimatsu et al. (2019) [10] discusses the phenomenon of two-phase flow in a horizontal sudden contraction pipe. This study observed how the contraction ratio affects the behavior of the water film using high-speed video analysis. Four flow regimes were observed after sudden contraction,

Ridwan Daris Naufal, Departement of Mechanical Engineering, Universitas Pembangunan Nasional Jakarta, Jakarta, 12450, Indonesia. E-mail: ridwandaris4502@gmail.com
Damora Rhakasywi, Departement of Mechanical Engineering, Universitas Pembangunan Nasional Veteran Jakarta, Jakarta, 12450, Indonesia. E-mail: rhakasywi@upnvj.ac.id
Fahrudin, Departement of Mechanical Engineering, Universitas Pembangunan Nasional Veteran Jakarta, Jakarta, 12450, Indonesia. E-mail: fahrudin@upnvj.ac.id

including two-dimensional and three-dimensional disturbance waves. The frequency of occurrence of these waves is studied under various air and water flow rate conditions.

Besides being affected by pressure, the cavitation phenomenon is also affected by temperature. The study by Sun et al. (2023) [11] explored the effect of water temperature on the cavitation phenomenon in viscoelastic pipes. This study shows that water temperature affects not only the saturated vapor pressure but also the intrinsic parameters of viscoelastic pipes. An increase in temperature leads to a larger cavitation cavity volume and a shorter cavity duration.

Previous studies have examined cavitation development in pipe systems ranging from visual observation of flow patterns after sudden contraction to numerical modeling of transient cavitation and energy analysis in viscoelastic pipes. However, most studies have only focused on a single pipe or a single diameter constriction, whether of gradual or sudden contraction. In certain conditions, such as those found in nuclear power plant cooling systems with pipe configurations featuring multiple sudden contractions, cavitation often occurs, potentially damaging the pipe structure and reducing system reliability. Therefore, this study is essential for providing a new understanding of cavitation formation in pipes with gradual and sudden contractions and for evaluating its mitigation through the addition of a fillet radius at the contraction area. The study was carried out numerically on pipes with diameters of D, 0.6D, and 0.4D, arranged in series, and the flow rate was varied between 500 and 3000 l/min to simulate the high flow rate conditions typical of cooling systems. Additionally, the effect of fillet radius variation on pressure distribution and cavitation was systematically investigated.

II. METHOD

This study was conducted to determine the formation of cavitation in a pipe series. The series pipe was simulated using a computational method with ANSYS Fluent software. The simulation includes pre-processing stages such as geometry and mesh creation, processing (solving), and post-processing such as verification and validation of simulation results. The computational process will be validated by comparing the analytical calculation results of the pressure drop generated along the pipe with the pressure drop from the simulation results.

A. Cavitation in Pipe Series

Cavitation is a phenomenon characterized by local vaporization due to a pressure drop to the saturation point of water vapor, accompanied by a massive increase in velocity resulting in the formation of a local cavity [12]. In series pipes, the pressure drop is caused by sudden and repeated contraction of the pipe diameter [13]. Pressure loss due to contraction is regulated by the pressure loss coefficient (K_{loss}) as determined by experiments [14]. The value of the pressure loss coefficient is plotted against the ratio of the pipe cross-sectional area in Figure 1. Additionally, pressure loss is generated by the roughness of the inner pipe wall [15]. It is supported by the Bernoulli equation in equation 1. Where f is derived from the relationship between the Reynolds number in equation 2, material roughness, and pipe diameter based on the Moody diagram [16]. To reduce the impact of pressure drop due to sudden contraction, a fillet shape is added at the contraction area. By doing so, the pressure change will affect the development of cavitation in the pipe.

$$\Delta p = 0.5\rho\left[(u_2^2 - u_1^2) + \sum_{n=1}^{3}\left(u_n f_n \frac{L_n}{D_n}\right) + \sum_{k=1}^{2}\left(u_{k+1}K_k\right)\right] \quad (1)$$

$$\mathrm{Re} = \frac{\rho u D}{\mu} \quad (2)$$

The potential for cavitation in a fluid flow can be determined by the cavitation number (σ) [2] Cavitation number is a non-dimensional value of the ratio of local pressure change to the fluid saturated vapor pressure to the fluid dynamic pressure [17], as shown in equation 3. Where p_v is the saturated vapor pressure of the fluid at a specific temperature obtained analytically using the Antoine equation at the experimental temperature [18], the constants that satisfy are as follows: A=8.07131, B=1730.68, C=233.426 in 27°C temperature condition [19] Under ideal conditions, cavitation is likely to occur when the cavitation number value falls within the range of < 0.5 [1], [6]. This number can change if the flow conditions contain impurities or dissolved gases [2].

$$\sigma = \frac{p - p_v}{0.5\rho u^2} \quad (3)$$

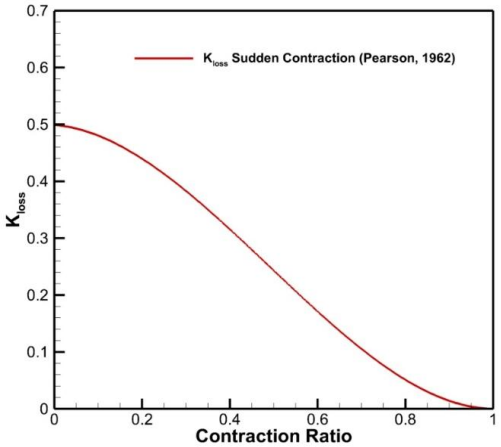

Figure. 1. Relationship of pressure loss coefficient to cross-sectional area ratio from experiments [14].

B. Computational Method

1) Pipe Geometry

The three pipes tested were arranged in series with a diameter ratio of D - 0.6D - 0.4D, and a diameter value of D = 50mm. The pipe lengths were 0.472 L, 0.310 L, and 0.219 L, respectively, with a total length of L = 7.11 m, ensuring the flow was fully developed before entering the contraction area. In addition to the sudden contraction, the fillet shape at the pipe joints was also tested, varying with radius R = 1 mm, R = 2 mm, and R = 4 mm, to determine the impact of the fillet shape and its radius magnitude on cavitation formation. An engineering drawing with boundary condition position is shown in Figure 2. In addition to making the computation time efficient, the pipe geometry is made in 2D with symmetry.

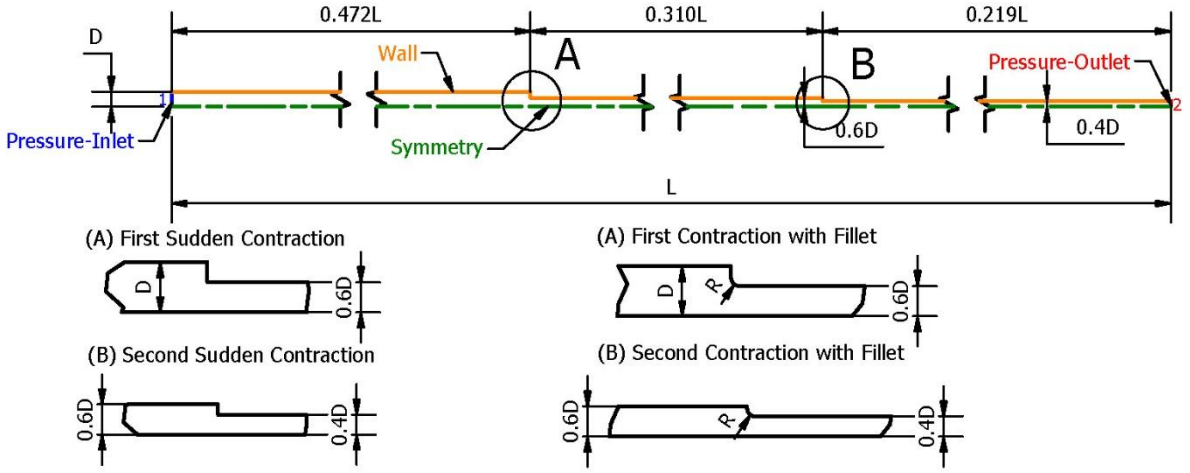

Figure. 2. Engineering drawing of a pipe with boundary condition position and its variations

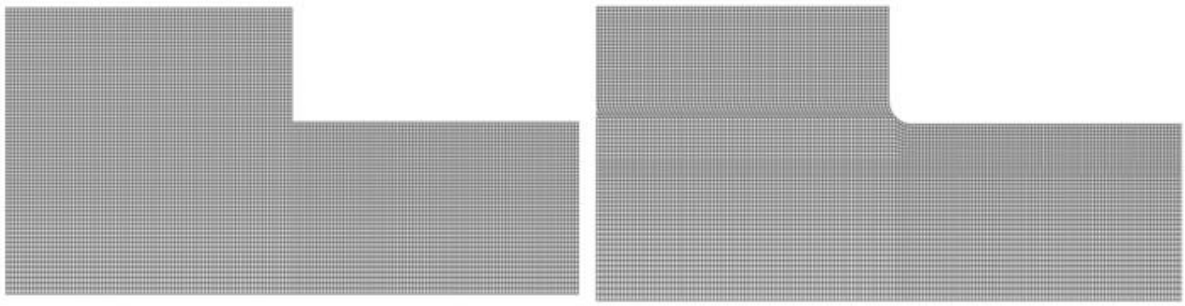

(a) (b)

Figure. 3. Quadrilateral Mesh in Contraction Area, (a) Sudden Contraction (b) Contraction with Fillet

2) Meshing

The meshing process is necessary in the computational process as it divides the geometry domain into small elements [20]. In addition, the meshing process also determines the efficiency of the computational process. For this reason, this study employed a quadrilateral mesh shape. This mesh shape has several advantages for the computational process in this study, including a low cost per iteration and suitability for simple geometry [21]. Additionally, the mesh is refined near the wall to achieve the best results for each phenomenon that forms in this region. The mesh geometry used in this study is illustrated in Figure 3.

3) Governing Equation

The numerical computing process uses the RANS governing equations to model and analyze fluid flow behavior. These equations include the continuity and momentum equations. The continuity equation in equation 4 describes the conservation of mass, while the momentum equation in equation 5 describes the

TABLE 1.
FLUID PROPERTIES

Fluid	Density (kg/m^3)	Dynamic viscosity (kg/m.s)
Water-Liquid	998.20	1.003×10^{-3}
Water-Vapor	0.0173	9.727×10^{-6}

conservation of momentum. Additionally, a turbulent model is necessary to estimate the complex turbulent flow. Therefore, this study uses the k-ε turbulent model in the numerical computation process. This turbulent model has the advantage of being suitable for flows with high Reynolds numbers [22]. The k-ε turbulent model consists of two equations: equation 6, which describes the turbulent kinetic energy, and equation 7, which describes the energy dissipation rate. The model constant were obtain from experiments: $C_{1\varepsilon} = 1.44$; $C_{2\varepsilon} = 1.92$; $C_\mu = 0.09$; $\sigma_k = 1.0$; $\sigma_\varepsilon = 1.3$.

$$\frac{\partial(\rho_m)}{\partial t} + \nabla.\left(\rho_m \vec{u}_m\right) = 0 \tag{4}$$

$$\frac{\partial\left(\rho_m \vec{u}_m\right)}{\partial t} + \nabla.\left(\rho_m \vec{u}_m \vec{u}_m\right) = -\nabla p + \nabla.\left[\mu_m\left(\nabla\vec{u}_m + \nabla\vec{u}_m^T\right)\right] + \rho_m \vec{g} + \vec{F} - \nabla.\left(\sum_{k=1}^{n} a_k \rho_k \vec{u}_{dr,k} \vec{u}_{dr,k}\right) \tag{5}$$

$$\frac{\partial(\rho k)}{\partial t} + \frac{\partial(\rho k u_i)}{\partial x_i} = \frac{\partial}{\partial x_j}\left[\left(\mu + \frac{\mu_t}{\sigma_k}\right)\frac{\partial k}{\partial x_j}\right] + G_k + G_b - \rho\varepsilon - Y_M + S_k \tag{6}$$

$$\frac{\partial(\rho\varepsilon)}{\partial t} + \frac{\partial(\rho\varepsilon u_i)}{\partial x_i} = \frac{\partial}{\partial x_j}\left[\left(\mu + \frac{\mu_t}{\sigma_\varepsilon}\right)\frac{\partial\varepsilon}{\partial x_j}\right] + C_{1\varepsilon}\frac{\varepsilon}{k}\left(G_k + C_{3\varepsilon}G_b\right) - C_{1\varepsilon}\rho\frac{\varepsilon^2}{k} + S_\varepsilon \tag{7}$$

The Zwart-Gerber-Belamri cavitation model was chosen in this study because it physically separates the evaporation process when the local pressure drops below the saturated vapor pressure ($p < p_v$), and the condensation process when the pressure rises above the vapor pressure ($p > p_v$) [23], as shown in equation 8. The model defines the mass transfer rate per unit volume based on the difference between local pressure and vapor pressure, the size of the nucleating bubbles, and the volume fraction of the vapor phase, thus describing the spatial distribution of cavitation in detail. The model equations used provide a value for the total interphase mass transfer rate due to cavitation per unit volume ($\dot{S}_{lv}$), which is relevant for evaluating the intensity of cavitation development and shrinkage in the sudden contraction zone of the pipe.

$$\dot{S}_{lv} = \begin{cases} F_{vap}\dfrac{3r_{nuc}(1-r_v)\rho_v}{R_B}\sqrt{\dfrac{2(p_v-p)}{3\rho_l}} \Rightarrow p < p_v \\ F_{cond}\dfrac{3r_v\rho_v}{R_B}\sqrt{\dfrac{2(p-p_v)}{3\rho_l}} \Rightarrow p > p_v \end{cases} \tag{8}$$

The model has been validated and demonstrates good performance for a wide range of liquids and devices with the following parameters: $R_B = 10^{-6}$ m; $r_{nuc} = 5 \times 10^{-4}$; $F_{vap} = 50$; and $F_{cond} = 0.01$ [23].

4) Boundary Condition

The boundary conditions are determined based on pressure-inlet, pressure-outlet, wall and symmetry. The pressure-inlet value is calculated from the variation in volume flow rate using the Bernoulli equation. Volume flowrate variations applied are 500, 1000, 1500, 2500, and 3000 l/m. On the other hand, the pressure-outlet is equipped with a zero-pressure gauge to represent water interacting with environmental pressure. For the roughness value on the wall, a uniform copper pipe material with a roughness of 1.5×10^{-6} m is used [24]. Additionally, the fluid properties used are water and water vapor, with a vaporization pressure of 3.54 kPa. The fluid properties are shown in Table 1.

5) Mesh Independence Test

The use of an appropriate mesh requires a verification process to ensure the mesh used is suitable. The mesh quality in this study is determined by the Richardson extrapolation method [25]. The mesh independence test process involves investigating three mesh qualities: fine, medium, and coarse meshes. The mesh quality is determined based on the number of elements tested. This study uses the following numbers of elements: 750,000 for fine mesh, 375,000 for medium mesh, and 187,500 for coarse mesh. Each change in the number of mesh elements is determined by a ratio of 2. The pressure parameter at the inlet is used to evaluate the verification results of each tested mesh.

TABLE 2.
MESH INDEPENDENCE TEST RESULT

Mesh Type	p_1 (kPa)	$\bar{\bar{p}}$	r	GCI_{fine}	GCI_{coarse}	$\frac{GCI_{fine}}{GCI_{coarse}r^p}$	Error (%)
Fine	412.81						0.014%
Medium	412.98	1.947	2	0.018%	0.0679%	1.000	0.054%
Coarse	413.62						0.210%

Following the same calculation step as Daris Naufal et al. (2025) [22], mesh independence test calculation results are obtained by considering a convergence range around ≈ 1. The following mesh independence test calculation results are shown in Table 2. The results of the mesh independence test calculation indicate that the fine mesh type yields the smallest error value. Thus, this study was conducted with a fine mesh type.

III. RESULTS AND DISCUSSION

A. Validation

The validation process involves comparing the results of analytical pressure drop calculations based on volume flow rate with the simulation results. It is done to ensure that the simulation data aligns with the actual conditions.

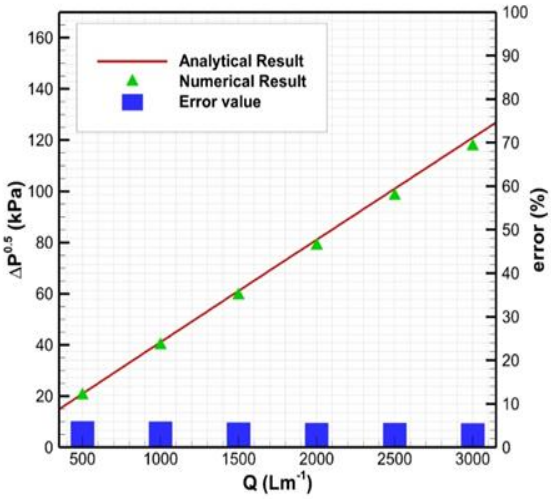

Figure. 4. Graph of pressure drop validation results against flow rate changes

The validation comparison graph is shown in Figure 4. It can be seen that the simulated pressure drop change rate is similar to the simulation results. Additionally, the results of analytical calculations and simulations yield an average error of approximately 5.74%. With an average error of less than 10%, it can be concluded that the simulation results are valid.

B. Effect of Fillet Radius on Pressure Distribution

The contour of the static pressure distribution in the first contraction area is shown in Figure 5. With high discharge variations, it is evident that there is a decrease in pressure in the area. The addition of fillets in the

contraction area has been proven to reduce the area of the low-pressure zone (vacuum region), which is a primary factor in the formation of cavitation. As the fillet radius increases, the flow transition becomes smoother, allowing the fluid acceleration not to change significantly. This results in an increase in the minimum pressure in the contraction area and a corresponding decrease in the overall pressure drop. The same phenomenon occurs in the second contraction area, as shown in Figure 6, characterized by lower pressure and a more pronounced pressure change gradient. It is due to the repeated pressure drop from the first contraction, and the second contraction being relatively minor. Therefore, the low-pressure zone (vacuum region) becomes more significant in the second contraction area. This result is consistent with Bernoulli's theory and the concept of flow separation. On the other hand, this finding also aligns with the research conducted by Nohmi et al. (2019) [26], who stated that the addition of fillets or chamfers is effective in reducing the risk of cavitation in narrowed flow systems.

.

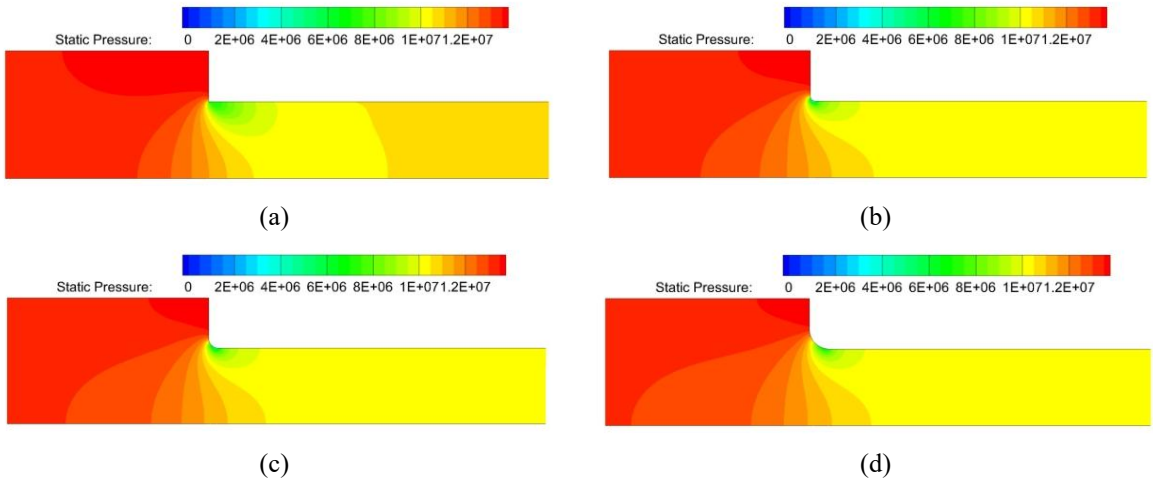

Figure. 5. First contraction pressure contour with 3000 l/m flow rate, (a) R = 0mm (b) R = 1mm (c) R = 2mm (d) R = 4mm

C. Effect of Fillet Radius on Cavitation Development

The cavitation number value generally characterizes the cavitation phenomenon in piping systems. The smaller the cavitation number value, the higher the potential for cavitation formation. In this study, the distribution analysis of cavitation numbers was carried out specifically in the area near the pipe joint wall. It is done to determine the tendency of the geometry transition zone, in the form of a sudden contraction, to produce significant pressure gradients due to sudden acceleration and flow separation. This condition often triggers the formation of a minimum pressure region around the contraction wall and becomes the critical point for cavitation.

As shown in the cavitation number distribution graph near the first contraction wall in Figure 7, the cavitation number values consistently exceed one across all variations of discharge and fillet radius. It indicates that the local static pressure in the area does not drop low enough to approach the saturation pressure of water vapor at the operating temperature, suggesting that the potential for cavitation formation is minimal at the first contraction and making this area relatively safe from cavitation-induced damage. This phenomenon is further supported by the vapor phase fraction contours in Figure 8, which show no significant accumulation of vapor along the contraction wall. These findings align with those of Zhang et al. (2019) [27], who reported that in sudden contraction pipe joints, the cavitation number tends to remain high when the contraction ratio is moderate. Their study found that only more extreme diameter reductions greater than 0.6 significantly increase flow acceleration, flow separation, and local static pressure drop, thereby raising the risk of cavitation. Since the first contraction in this study uses a 0.6 contraction ratio, it does not induce pressure drops near the vapor pressure threshold, further confirming the absence of cavitation in this region.

The distribution of cavitation number values in the near-wall area at the two contraction points shows significant differences in characteristics. In the 0.4 contraction ratio configuration during the second contraction, the cavitation number distribution data exhibited a more pronounced pattern. With a low discharge of 500 l/m, the lowest cavitation number value is recorded below 0.5 without a fillet radius, and it progressively increases with an increasing fillet radius until it reaches a safer value close to 1. This condition indicates that the fillet radius effectively reduces the sudden acceleration of the flow and decreases the intensity of the local pressure depression, thereby reducing the potential for cavitation formation.

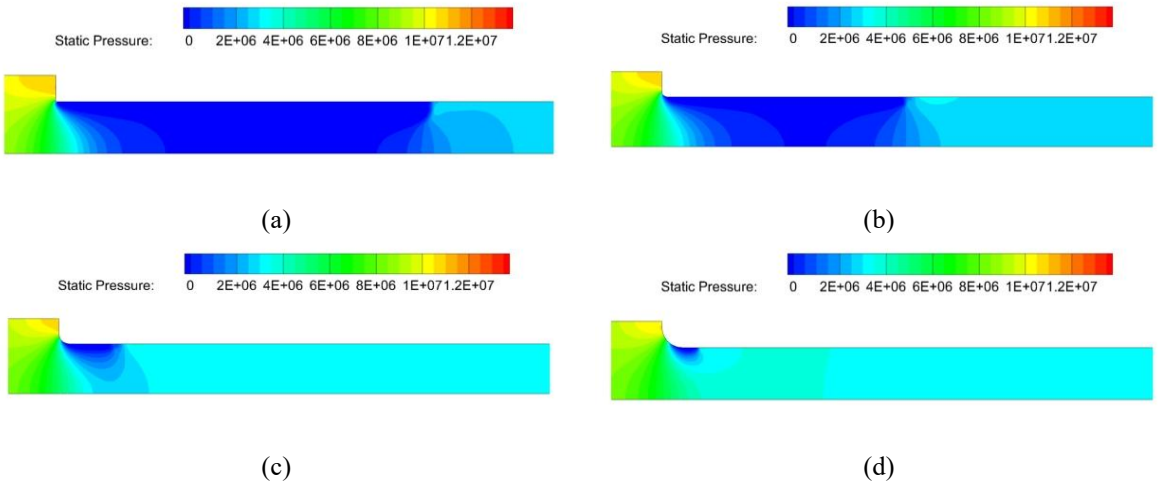

Figure. 6. Second contraction pressure contour drawing with 3000 l/m flow rate, (a) R = 0mm (b) R = 1mm (c) R = 2mm (d) R = 4mm

With higher discharges in the range of 1000 to 3000 l/m, the cavitation number in the second contraction area even reaches a value close to or equal to zero. This phenomenon is reflected in the distribution graph, which shows a cavitation number ≈ 0 zone that becomes longer as the applied discharge increases. This condition occurs due to an increase in flow velocity and dynamic pressure, along with an increase in applied discharge. The addition of fillet radius in the second contraction area significantly shortens the length of the low cavitation number zone. It indicates the role of the fillet geometry in dampening the acceleration gradient and reducing the potential for cavitation. This difference confirms that the second contraction area is a critical location for cavitation formation due to the combination of greater flow acceleration and a more drastic diameter ratio, while the first contraction tends to be safe against cavitation risk. It supports the research of Zhang et al. (2019) [27], which showed the relationship between diameter constriction ratio and pressure depression, as well as the study of Nohmi et al. (2019) [26] that verified the effectiveness of fillet radius in reducing the minimum pressure intensity in sudden contraction pipe joints.

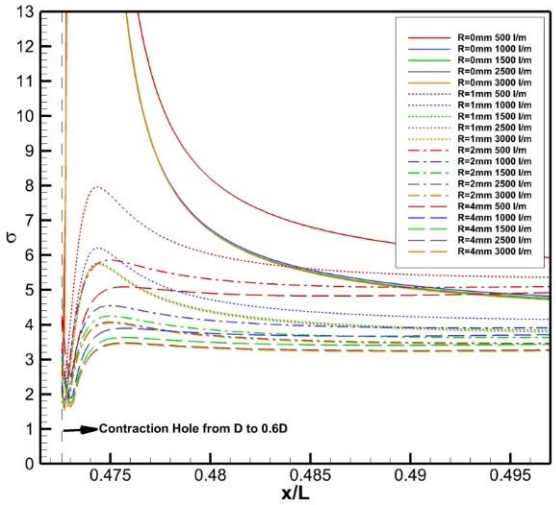

Figure. 7. Cavitation number distribution graph near the wall in the first contraction

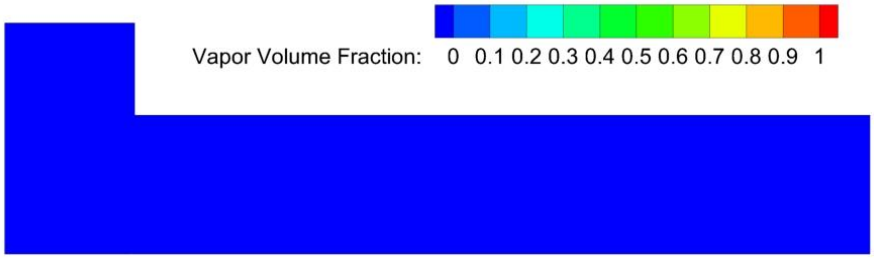

Figure. 8. Vapor volume fraction contour at the first sudden contraction (R=0) at 3000 l/m flow rate

The contour distribution of vapor volume fraction at the second contraction with a 3000 Lpm flow rate, shown in Figure 10, provides visual validation of the tendency for cavitation formation that was previously predicted through cavitation number analysis. The simulation results show that, in the variation without a fillet radius (R = 0 mm), the maximum vapor volume fraction value is relatively larger than in all geometry variations with a fillet radius. With the addition of fillets in the contraction area, it can be observed that the larger the fillet radius applied, the smaller the value of the vapor volume fraction formed tends to be. It is because the fillet radius acts as a geometrical diffuser, smoothing the cross-sectional changes and effectively reducing the fluids acceleration speed in the contraction area. Therefore, it indicates that without the dampening of the acceleration gradient by the fillet, the flow experiences a more extreme pressure drop, causing the local pressure to fall below the fluids saturated vapor pressure and leading to the conversion of part of the liquid fluid into the vapor phase. Additionally, the fillet radius also reduces the intensity of flow separation and local turbulence, two factors closely related to the formation of cavitation bubbles.

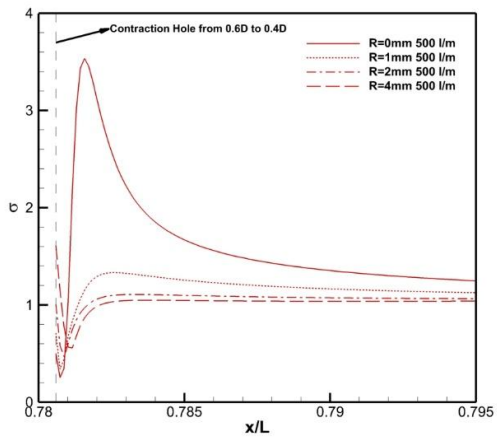

(a)

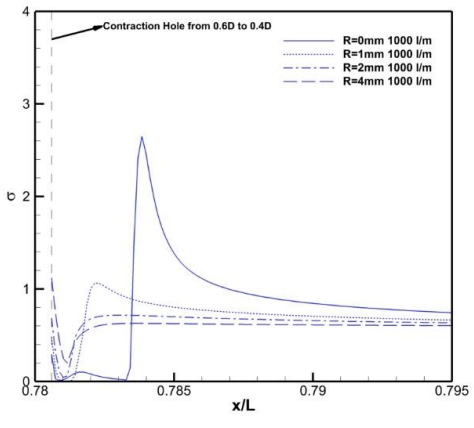

(b)

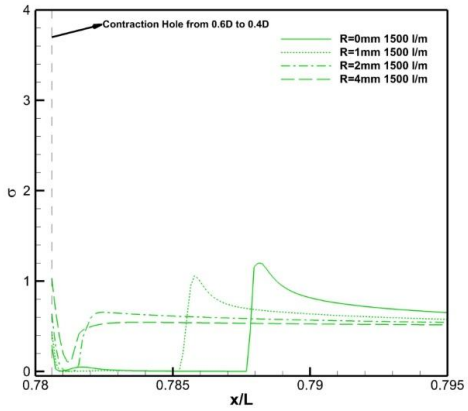

(c)

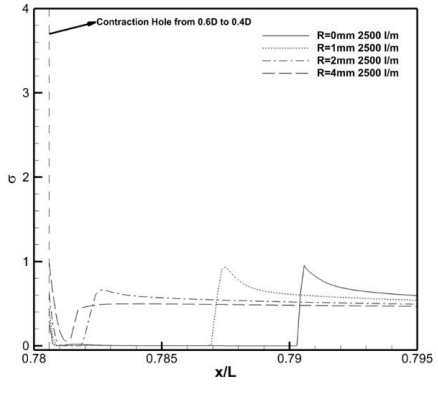

(d)

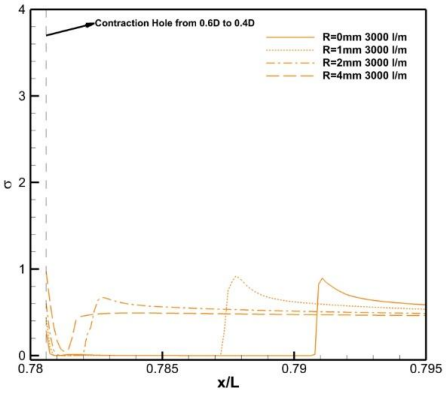

(e)

The graphs in Figure 11a show that increasing discharge raises the peak vapor fraction due to higher flow acceleration and local pressure drops. Without a fillet radius, the maximum vapor fraction approaches one at the highest discharge, indicating intense cavitation with potential for pipe damage. As the fillet radius increases, both the peak vapor fraction and the cavitation zone length decrease significantly, as also illustrated in Figure 11b. It demonstrates that the volume and extent of cavitation are reduced by smoother joint geometry, which raises minimum static pressure and minimizes wake regions and downstream vortices. These results align with flow reattachment principles, where the fillet reduces separation and increases local pressure, limiting cavitation growth. Therefore, increasing the fillet radius effectively mitigates cavitation formation. This finding is consistent with that of Nohmi et al. (2019), who reported that fillets significantly decrease cavity length and the impact of bubble implosion.

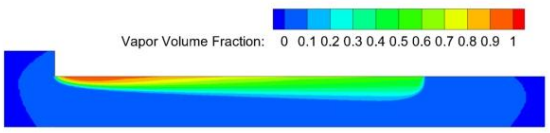

(a)

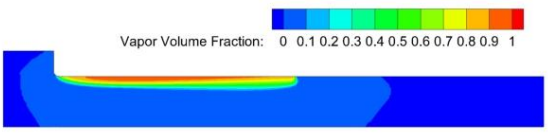

(b)

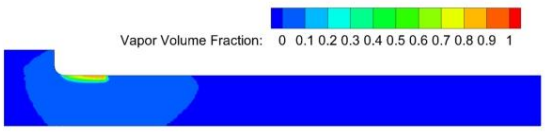

(c)

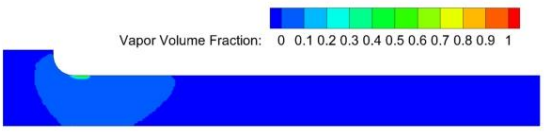

(d)

Figure. 10. Vapor volume fraction contour with 3000 l/m discharge at the second contractio*n*, (a) R = 0mm (b) R = 1mm (c) R = 2mm (d) R = 4mm

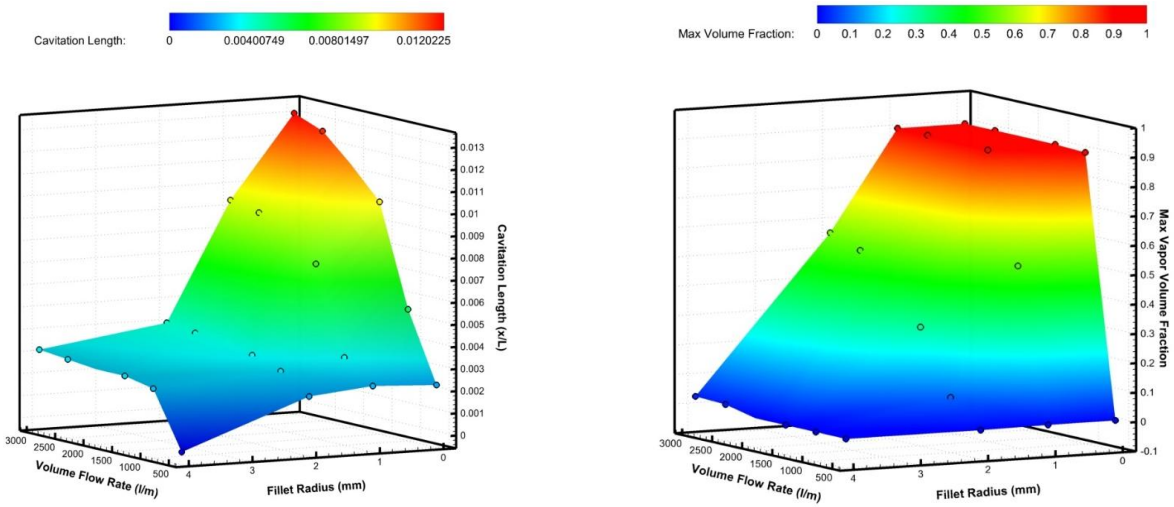

(a) (b)

Figure. 11. Graph showing the relationship between flow rate, fillet radius, and (a) Cavitation length (b) Max Vapor Volume Friction

V. CONCLUSION

This study numerically analyzed cavitation in a series pipe system with abrupt contractions at diameter ratios of D, 0.6D, and 0.4D, varying fillet geometry and flow rates from 500 to 3000 l/min. The first contraction showed minimal cavitation risk, with cavitation numbers consistently above 0.5 and no significant vapor accumulation. In contrast, the second contraction exhibited cavitation numbers approaching zero at high discharge, leading to elongated cavitation zones along the wall. Flow rate was the dominant factor in increasing the vapor fraction and the length of the cavitation zone, demonstrating the relationship between flow acceleration and local pressure depression. Adding fillets effectively raised cavitation numbers, shortened cavitation zones, and reduced vapor fractions, confirming joint geometry as a primary mitigation strategy. The strong correlation between low cavitation number and high vapor fraction validates cavitation number as a predictive indicator. Overall, these findings offer valuable insights for designing more reliable industrial piping systems that are resistant to cavitation damage

REFERENCES

[1] P. Braeutigam, M. Franke, Z. L. Wu, and B. Ondruschka, "Role of different parameters in the optimization of hydrodynamic cavitation," *Chem. Eng. Technol.*, vol. 33, no. 6, pp. 932–940, 2010, doi: 10.1002/ceat.201000021.

[2] Q. Li, C. Zong, F. Liu, T. Xue, A. Zhang, and X. Song, "Numerical and experimental analysis of the cavitation characteristics of orifice plates under high-pressure conditions based on a modified cavitation model," *Int. J. Heat Mass Transf.*, vol. 203, Apr. 2023, doi: 10.1016/j.ijheatmasstransfer.2022.123782.

[3] P. Tang, J. M. Juárez, and H. Li, "Investigation on the effect of structural parameters on cavitation characteristics for the venturi tube using the CFD method," *Water (Switzerland)*, vol. 11, no. 10, Oct. 2019, doi: 10.3390/w11102194.

[4] J. ZHANG, Q. YANG, Y. WANG, W. XU, and J. CHEN, "Experimental investigation of cavitation in a sudden expansion pipe," *J. Hydrodyn. Ser. B*, vol. 23, no. 3, pp. 348–352, 2011, doi: https://doi.org/10.1016/S1001-6058(10)60122-9.

[5] H. Shi, M. Li, P. Nikrityuk, and Q. Liu, "Experimental and numerical study of cavitation flows in venturi tubes: From CFD to an empirical model," *Chem. Eng. Sci.*, vol. 207, pp. 672–687, 2019, doi: https://doi.org/10.1016/j.ces.2019.07.004.

[6] Qing Yang *et al.*, "Experimental and Eulerian-Lagrangian numerical investigation on cavitation erosion characteristics in venturi pipes with different divergent angles," *Ultrason. Sonochem.*, Feb. 2025, doi: 10.1016/j.ultsonch.2025.107278.

[7] H. Ghassemi and H. F. Fasih, "Application of small size cavitating venturi as flow controller and flow meter," *Flow Meas. Instrum.*, vol. 22, no. 5, pp. 406–412, Oct. 2011, doi: 10.1016/j.flowmeasinst.2011.05.001.

[8] X. Tang, X. Duan, H. Gao, X. Li, and X. Shi, "CFD investigations of transient cavitation flows in pipeline based on weakly-compressible model," *Water (Switzerland)*, vol. 12, no. 2, Feb. 2020, doi: 10.3390/w12020448.

[9] G. Lei *et al.*, "Influence of the transition section shape on the cavitation characteristics at the bottom outlet," *Water Supply*, vol. 23, no. 8, pp. 3061–3077, Jul. 2023, doi: 10.2166/ws.2023.181.

[10] T. Fujimatsu, M. Kito, and K. Kondo, "Two-phase flow phenomena in a horizontal pipe with a sudden contraction: Effects of contraction ratio on film behaviour," in *WIT Transactions on Engineering Sciences*, WITPress, 2019, pp. 53–62. doi: 10.2495/MPF190061.

[11] Q. Sun, F. Wang, Y. Bin Wu, Y. Xu, and Y. Hao, "Energy analysis of transient flow with cavitation by considering the effect of water temperature in viscoelastic pipes," *J. Hydroinformatics*, vol. 25, no. 5, pp. 2034–2052, Sep. 2023, doi: 10.2166/hydro.2023.231.

[12] X. LUO, B. JI, and Y. TSUJIMOTO, "A review of cavitation in hydraulic machinery," *J. Hydrodyn. Ser. B*, vol. 28, no. 3, pp. 335–358, 2016, doi: https://doi.org/10.1016/S1001-6058(16)60638-8.

[13] V. V. R. Kaushik, S. Ghosh, G. Das, and P. K. Das, "CFD simulation of core annular flow through sudden contraction and expansion," *J. Pet. Sci. Eng.*, vol. 86–87, pp. 153–164, May 2012, doi: 10.1016/j.petrol.2012.03.003.

[14] J. R. A. Pearson, "Handbook of Fluid Dynamics. Edited by V. L. STREETER. McGraw-Hill, 1961. 1215pp. £9. 6s.," *J. Fluid Mech.*, vol. 14, no. 4, pp. 630–631, 1962, doi: DOI: 10.1017/S0022112062211494.

[15] K. Huang, J. Wan, C. Chen, Y. Q. Li, D. Mao, and M. Y. Zhang, "Experimental investigation on friction factor in pipes with large roughness," *Exp. Therm. Fluid Sci.*, vol. 50, pp. 147–153, Oct. 2013, doi: 10.1016/j.expthermflusci.2013.06.002.

[16] L. Del Frate, F. Moretti, G. Galassi, and F. D'Auria, "Limitations in the Use of the Equivalent Diameter," *World J. Nucl. Sci. Technol.*, vol. 06, no. 01, pp. 53–62, 2016, doi: 10.4236/wjnst.2016.61005.

[17] Y. Liu and B. Li, "Numerical Investigation of the Cavitation Characteristics in Venturi Tubes: The Role of Converging and Diverging Sections," *Appl. Sci.*, vol. 13, no. 13, 2023, doi: 10.3390/app13137476.

[18] E. Sanjari, M. Honarmand, H. Badihi, and A. Ghaheri, "An accurate generalized model for predict vapor pressure of refrigerants," *Int. J. Refrig.*, vol. 36, no. 4, pp. 1327–1332, 2013, doi: https://doi.org/10.1016/j.ijrefrig.2013.01.007.

[19] M. N. F. Rachman, D. Rhakasywi, and F. Fahrudin, "Numerical Study of Cavitation Phenomenon in a Venturi Tube," *J. La Multiapp*, vol. 5, no. 4, pp. 453–464, Aug. 2024, doi: 10.37899/journallamultiapp.v5i4.1432.

[20] M. F. Lukiano, J. Julian, F. Wahyuni, and W. Iskandar, "The Influence of Mounting Angle on Gurney Flap on The

Aerodynamics Performance of NACA 0015 Using CFD Method," 2023.

[21] R. Fariansyah Billad, J. Julian, F. Wahyuni, W. Iskandar, D. Nely, and T. Bunga, "Numerical Modelling of NACA 0015 Airfoil Under the Erosion Condition Pemodelan Numerik Airfoil NACA 0015 Dalam Kondisi Erosi," vol. 6, pp. 133–142, 2024.

[22] R. Daris Naufal, J. Julian, F. Wahyuni, R. Hendra Purba, and N. Toding Bunga, "The Utilization of Single and Double Orifice Plates in Pipe Inner Flow Structure by Computational Method Pemanfaatan Pelat Orifice Tunggal dan Ganda pada Struktur Aliran dalam Pipa dengan Metode Komputasi," vol. 7, no. 1, 2025.

[23] T. Belamri, P. J. Zwart, and A. G. Gerber, "A two-phase flow model for predicting cavitation dynamics," 2004.

[24] J. A. Marshall, "Measuring copper surface roughness for high speed applications," in *Proc. IPC*, 2015, pp. 1–6.

[25] P. J. R. And and P. M. Knupp, "COMPLETED RICHARDSON EXTRAPOLATION," 1993.

[26] M. Nohmi, S. Kagawa, T. Tsuneda, W. Tsuru, and K. Yokota, *Numerical Analysis of Contraction Geometry Effects on Cavitation Choking in a Piping System*. 2019. doi: 10.1115/AJKFluids2019-5359.

[27] T. Zhang, R. X. Hao, X. Q. Zheng, and Z. Zhang, "Effect of the area contraction ratio on the hydraulic characteristics of the toothed internal energy dissipaters," *Water (Switzerland)*, vol. 11, no. 7, Jul. 2019, doi: 10.3390/w11071406.